# Estimation of Nozzle Throat Wall Temperature History in Hybrid Rockets

Landon KAMPS[*1], Harunori NAGATA[*2]

**ABSTRACT**

The causes and prevention measures of nozzle throat erosion in hybrid rockets is currently an important topic of research in the hybrid rocket community. It is widely accepted that erosion rates will depend on the nozzle wall temperature, however the lack of a sufficient measurement technique has prevented the collection of experimental results. This study introduces an iterative procedure for estimating the wall temperature and heating rate from the typical experimental measurements of pressure, (inner) nozzle temperature and flowrate, and reveals that the convective heat transfer coefficient at the nozzle throat may reach 2 times the value predicted by the Bartz correlation.

**Keywords:** Nozzle Erosion, Temperature Estimation, Heat Flux

**概要**

ノズル侵食の原因は、ハイブリッドロケット開発における重要な研究テーマである。浸食速度はノズル壁面温度に依存することが広く知られているが、実験データの収集が困難である。本研究では、計測可能な実験値である圧力、ノズル内部温度および酸化剤流量から壁面温度および熱伝達率を推定するための収束計算を導入する。その結果、侵食が発生する場合のノズルスロートにおける熱伝達率は Bartz 方程式によって得られる値の 2〜3 倍になることが予測された。

## 1. INTRODUCTION

The estimation of temperatures within the nozzle and at the nozzle surface during operation of a chemical rocket is essential for the selection of an appropriate nozzle material and design. Two particularly important design considerations are erosion at the nozzle throat due to heterogenous surface reactions, referred to as nozzle erosion, and the structural failure of nozzle materials due to thermal stress. Whereas an abundance of research and development has been carried out on nozzle material selection for overcoming thermal stress, there are very few experimental reports addressing the topic of nozzle erosion. Despite a general understanding that hybrid rockets are more prone to thermochemical erosion than their liquid or solid rocket counterparts [1]-[3], there only a few studies that directly address nozzle erosion in hybrid rocket configurations.

With the recent introduction of a method for estimating nozzle throat erosion and oxidizer-to-fuel mass ratio histories in hybrid rockets, titled Nozzle Throat Reconstruction Technique or NTRT, it is now possible to collect experimental data for nozzle erosion rates [3]. However, without corresonding experimental values for nozzle throat wall temperature it is impossible to incoporate heterogeneous combustion theory into the resulting empirical model and correlations. This is evident in Fig. 1 which was reported by Kamps et al. [3]. In Fig. 1, there appears to be a sharp decrease in erosion rates in the direction of decreasing equivalence ratio (0.5-0.7) even though the concentration of oxidants in the combustion gas is expected to increase in this region. It is possible, for example, that this phenomenon could have been explained had information about wall temperature been included in the correlation. The reason for this is that the heterogeneous surface reaction rates of oxidizing species in the combustion gas with the nozzle wall $\dot{r}_i$ are known to follow the Arrhenius equation [2][4]-[6].

$$\dot{r}_i = k_j P_i^{n_j} = \frac{A_j T_w^{b_j} P_i^{n_j}}{\rho_n \exp\left(E_j / R_u T_w\right)} \tag{1}$$

where the subscripits *i* and *j* represent the oxidizing species (predominately $CO_2$, $H_2O$, $O_2$, OH and O) and

This document is provided by JAXA.

corresponding chemical reaction carbon, and the constants $A_j$, $E_j$, $b_j$ and $n_j$ are determined empirically. The term $R_u$ is the universal gas constant (8.314 J/mol-K), $\rho_n$ is the nozzle density (1850 kg/m$^3$ in this study), and the term $P_i$ is the partial pressure of species $i$ in the combustion gas.

The objective of this research is to propose a method for estimating nozzle throat wall temperature history using the results of the NTRT and experimental measurements of temperature from within the nozzle with the aim of enabling experimental investigations of nozzle erosion based on heterogenous chemical reaction theory.

## 2. METHOD

### 2.1. Throat Wall Temperature Estimation Concept

The method for estimating nozzle throat wall temperature developed in this research is essentially a follow-on procedure to the NTRT. The concept is that heat transfer theory can be applied to the nozzle only because the time history of oxidizer-to-fuel mass ratio $\xi$ is available. This is because the combustion gas temperature, which drives the heat transfer process in the nozzle, along with the viscocity, density and Prandtl number are decided by $\xi$. A computation flowchart of this concept is summarized in Fig. 2, where experimental data for the histories of oxidizer mass flowrate, thrust and chamber pressure are input to the NTRT and the throat erosion and $\xi$ are output. These outputs continue on as intputs to the temperature estimation procedure which outputs the throat wall temperature and heat flux histories.

In following with the NTRT, which is an iterative procedure that equates experimental and theoretical values of characteristic exhaust velocity and thrust through the non-dimensional terms of combustion efficiency and thrust correction factor, the nozzle wall temperature estimation is also an iterative procedure that equates theoretical calculations of heat transfer to experimental measurements of temperature through non-dimensional terms. The first non-dimensional term $\zeta$, referred to as the heat transfer coefficient factor, is the ratio of the convective heat transfer coefficient at the nozzle throat to the value predicted by the Bartz correlation [7] : $\zeta = h/h_{\mathrm{Bartz}}$. The second non-dimensional term $\theta$, referred to as the wall temperature factor, is the ratio of the nozzle wall temperature to the combustion gas temperature at the throat : $\theta = T_w/T_g$. The third non-dimensional term $\phi$, referred to as partial pressure factor, is the ratio of the mole fraction of species $i$ at the nozzle wall to that in the bulk fluid : $\phi = X_{i,w}/X_{i,g}$.

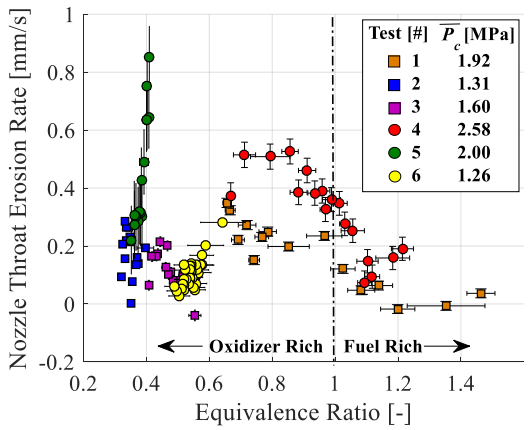


Fig. 1. Nozzle erosion rate correlation [3]

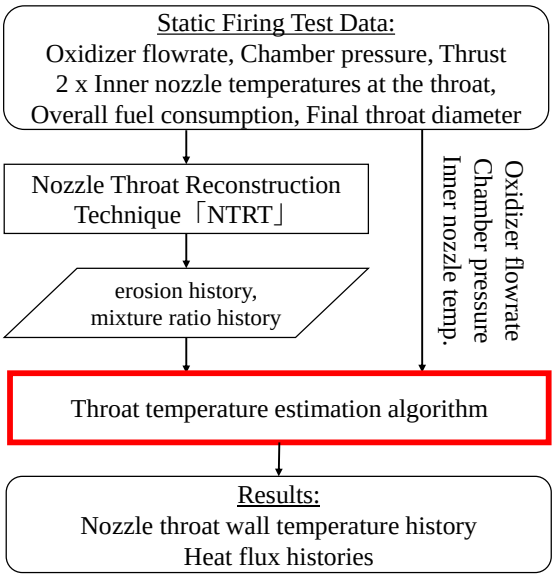


Fig. 2. Computational flowchart

### 2.2. Governing Equations

Convective, conductive and chemical heat flux in units of W/m$^2$, can be presented as functions of

This document is provided by JAXA.

non-dimensional terms $\zeta$, $\theta$, and $\phi$ as follows :

$$\dot{q}_{conv}\left(\zeta,\theta\right)=h_{Bartz}\zeta T_g\left(1-\theta\right)=\frac{\left[\frac{0.004186}{D_t^{0.2}}\left(\frac{\mu^{0.2}c_p}{\mathrm{Pr}^{0.6}}\right)\left(\frac{P_c g}{c^*}\right)\left(\frac{D_t}{r_c}\right)^{0.1}\right]}{\left[\frac{1}{2}\frac{T_w}{T_c}\left(1+\frac{\gamma-1}{2}\right)+\frac{1}{2}\right]^{0.68}\left[1+\frac{\gamma-1}{2}\right]^{0.12}}\zeta T_g\left(1-\theta\right) \tag{2}$$

$$\dot{q}_{cond}\left(\theta\right)\cong\frac{k}{\Delta r}\left(T_g\theta-T_{w+\Delta r}\right) \tag{3}$$

$$\dot{q}_{chem}\left(\phi\right)=\rho_n\sum\dot{r}_i H_{rxn,j}=\sum\frac{A_j T_w^{b_j}\left(\phi X_{i,g}P_c\right)^{n_j}}{\exp\left(E_j/R_u T_w\right)}H_{rxn,j} \tag{4}$$

In Eq. (2) the term $D_t$ is the nozzle throat diameter in units of m, $\mu$ is kinematic viscocity in units of Pa-s, $c_p$ is specific heat in units of J/kg-K, Pr is the Prandtl number, $P_c$ is the chamber pressure in units of Pa, $g$ is gravitational acceleration in units of m/s$^2$, $c^*$ is charateristic exhaust velocity in units of m/s, $r_c$ is the radius of curvature at the throat in units of m, $T_c$ is combustion gas temperature in units of K, and $\gamma$ is the specific heat ratio. The values of $\mu$, $c_p$, Pr, $c^*$, $\gamma$, and $T_c$, which are terms from the Bartz correlation [7], can be calculated using NASA CEA for a given $P_c$ and $\xi$ [8].

In Eq. (3) the term $k$ is thermal conductivity in units of W/m-K. In order to solve for the temperature term $T_{w+\Delta r}$ on the right-hand side of Eq. (3), the radial temperature profile at the nozzle throat plane must be solved. This is done by making the approximation that transient conduction in the nozzle is one-dimensional in the radial direction. Approximating the partial derivatives in the heat equation in cylindrical coordinates by the first term of the Taylor series expansion allows for us to solve for the radial temperature profile (i.e. the temperature at every $i$-th node) at the throat plane at time step $j$+1 based on the value at time step $j$ according to Eq. (5). A graphical depiction of the mesh used for this numerical calculation is shown in Fig. 3.

$$\begin{bmatrix} T_{w+\Delta r}^{j+1} \\ T_{w+2\Delta r}^{j+1} \\ \vdots \\ T_{r_{n2}-2\Delta r}^{j+1} \\ T_{r_{n2}-\Delta r}^{j+1} \end{bmatrix} = \begin{bmatrix} b_{w+\Delta r}^j & c_{w+\Delta r}^j & 0 & 0 & 0 \\ a_{w+2\Delta r}^j & b_{w+2\Delta r}^j & c_{w+2\Delta r}^j & 0 & 0 \\ 0 & \ddots & \ddots & \ddots & 0 \\ 0 & 0 & a_{r_{n2}-2\Delta r}^j & b_{r_{n2}-2\Delta r}^j & c_{r_{n2}-2\Delta r}^j \\ 0 & 0 & 0 & a_{r_{n2}-\Delta r}^j & b_{r_{n2}-\Delta r}^j \end{bmatrix}^{-1} \begin{bmatrix} a_{w+\Delta r}^j T_{w+\Delta r}^j \\ a_{w+2\Delta r}^j T_{w+2\Delta r}^j \\ \vdots \\ a_{r_{n2}-2\Delta r}^j T_{r_{n2}-2\Delta r}^j \\ a_{r_{n2}-\Delta r}^j T_{r_{n2}-\Delta r}^j \end{bmatrix} - \begin{bmatrix} a_{w+\Delta r}^j T_g \theta^j \\ 0 \\ \vdots \\ 0 \\ c_{r_{n2}-\Delta r}^j T_{n2}^j \end{bmatrix}$$

$T_w$ at $j+1$ Stiffness Matrix $T_w$ at $j$ Boundary (5)

$$a_i^j = 2\alpha^j r_i \Delta t - \alpha \Delta r \Delta t$$
$$b_i^i = -(4\alpha^j r_i \Delta t + 2 r_i \Delta r^2)$$
$$c_i^j = \alpha^j \Delta r \Delta t + 2\alpha^j r_i \Delta t$$
$$d_i = 2 r_i \Delta r^2$$

here $\Delta r$ is radial spacing of a computational mesh at the nozzle throat plane in units of m, $T_{w+\Delta r}$ is the temperature at the computational node closest to the nozzle throat surface in units of K, $\alpha$ is thermal diffusivity in units of m$^2$/s, and the subscript *n2* denotes the radial position of a thermocouple placed within the nozzle at the throat plane. The thermocouple couple temerapture history at this position is the term $T_{n2}$ in Eq. (5), which serves as a boundary condition. The other bounday in Eq. (5) is the solution for nozzle throat wall temperature history $T_w = T_g\theta$. It is important to point out that the thermal diffusivity and thermal conductivity of graphite are both functions of temperature. Since this data was not available for the graphite material used in this study, the results of research on the properties of graphite of similar densities (1800-1900 kg/m$^3$) were approximated with non-linear curve fits for this study [9][10]. The functions used in this study are ploted in Fig. 4.

This document is provided by JAXA.

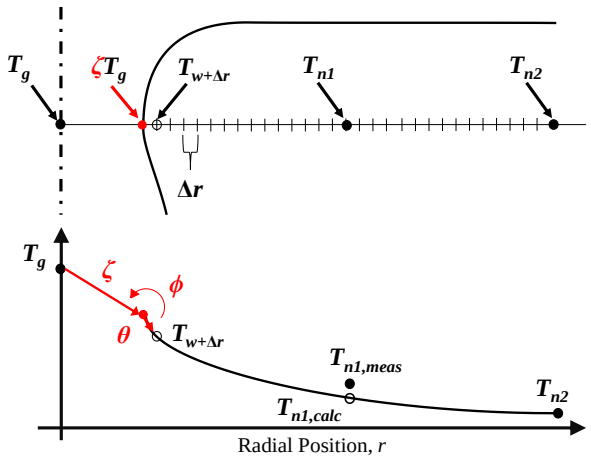


Fig. 3. Radial mesh for temperature calculations

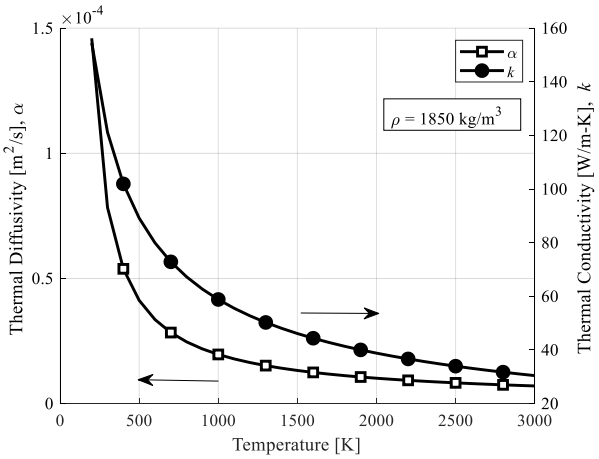


Fig. 4. Thermal properites of graphite

In Eq. (4), the term $H_{rxn,j}$ is the heat of reaction of the $j$-th reaction in units of J/kg(C). These values are functions of temperature, and are calculated using reference data for enthalpies listed in Ref. [11]. The five oxidizing species, the chemical equations of their reactions with graphite, and the corresponding Arrehnius constants are summarized in Table 1. According to Bianchi and Nasuti [2], one exception to the Arrhenius equation (Eq. (1) and the far right-hand term in Eq. (4)) should be made for reactions between diatomic oxygen and graphite. In this case, Eq. (6) should be considered.

**Table 1. Heterogeneous rate constants and reaction order with graphite [2]**

| $i$ | Species | Reaction | $j$ | $A_j$ | $E_j$, J/mol | $b_j$ | $n_j$ |
|---|---|---|---|---|---|---|---|
| 1 | $H_2O$ | $C_s + H_2O \rightarrow CO + H_2$ | 1 | 4.8E5 | 288E3 | 0.0 | 0.5 |
| 2 | $CO_2$ | $C_s + CO_2 \rightarrow 2CO$ | 2 | 9.0E3 | 285E3 | 0.0 | 0.5 |
| 3 | OH | $C_s + OH \rightarrow CO + H$ | 3 | 3.61E2 | 0.0 | -0.5 | 1.0 |
| 4 | O | $C_s + O \rightarrow CO$ | 4 | 6.655E2 | 0.0 | -0.5 | 1.0 |
| 5 | $O_2$ | $C_s + \frac{1}{2} O_2 \rightarrow CO$ | 5a | 2.4E3 | -125.6E3 | 0.0 | 0.0 |
| | | | 5b | 2.13E1 | -17.17E3 | 0.0 | 0.0 |
| | | | 5c | 5.35E-1 | 63.64E3 | 0.0 | 0.0 |
| | | | 5d | 1.81E7 | 406.1E3 | 0.0 | 0.0 |

Note: coincides with units of $P$ [atm] in Eqs. (1) and (4)

$$\rho_n \dot{r}_{O_2} = \left( \frac{k_{5a} p_{O_2} Y}{1 + k_{5b} Y} \right) + k_{5c} p_{O_2} (1 - Y) \quad \text{where} \quad Y = \left( 1 + \frac{k_{5d}}{k_{5c} p_{O_2}} \right)^{-1} \tag{6}$$

The Newton-Raphson method is used to iterate for the solution to the non-dimensional terms $\zeta$, $\theta$, and $\phi$. This requires minimizing the following three computational residual equations :

$$\psi_q = 1 - \frac{\dot{q}_{cond}}{\dot{q}_{conv}} - \frac{\dot{q}_{chem}}{\dot{q}_{conv}} \tag{7}$$

$$\psi_T = 1 - \frac{T_{n1,calc}}{T_{n1,meas}} \tag{8}$$

$$\psi_{\dot{r}} = 1 - \frac{\dot{r}_{calc}}{\dot{r}_{meas}} \tag{9}$$

Where the subscripts *meas* and *calc* distunguish experimentally measured values from the corresponding theoretical calculation, and $T_{n1}$ is the temperature at the position of a thermocouple placed closer to the nozzle throat than $T_{n2}$ in units of K. In other words, two thermocouple measurements at different distances from the

This document is provided by JAXA.

nozzle throat are necessary. The matrix inversion expressed by Eq. (10) is used to iterate for the solutions to the non-dimensional terms at every time :

$$\begin{bmatrix} \zeta^{i+1} \\ \theta^{i+1} \\ \phi^{i+1} \end{bmatrix} = \begin{bmatrix} \frac{\partial \psi_q^i}{\partial \zeta} & \frac{\partial \psi_q^i}{\partial \theta} & \frac{\partial \psi_q^i}{\partial \phi} \\ \frac{\partial \psi_T^i}{\partial \zeta} & \frac{\partial \psi_T^i}{\partial \theta} & \frac{\partial \psi_T^i}{\partial \phi} \\ \frac{\partial \psi_{\dot{r}}^i}{\partial \zeta} & \frac{\partial \psi_{\dot{r}}^i}{\partial \theta} & \frac{\partial \psi_{\dot{r}}^i}{\partial \phi} \end{bmatrix}^{-1} \begin{bmatrix} -\psi_q^i + \zeta^i \frac{\partial \psi_q^i}{\partial \zeta} + \theta^i \frac{\partial \psi_q^i}{\partial \theta} + \phi^i \frac{\partial \psi_q^i}{\partial \phi} \\ -\psi_T^i + \zeta^i \frac{\partial \psi_T^i}{\partial \zeta} + \theta^i \frac{\partial \psi_T^i}{\partial \theta} + \phi^i \frac{\partial \psi_T^i}{\partial \phi} \\ -\psi_{\dot{r}}^i + \zeta^i \frac{\partial \psi_{\dot{r}}^i}{\partial \zeta} + \theta^i \frac{\partial \psi_{\dot{r}}^i}{\partial \theta} + \phi^i \frac{\partial \psi_{\dot{r}}^i}{\partial \phi} \end{bmatrix} \tag{10}$$

until the convergence criteria expressed in Eq. (11) is satisfied.

$$\Psi = \sqrt{\psi_q^2 + \psi_T^2 + \psi_{\dot{r}}^2} < 10^{-3} \tag{11}$$

The superscript *i* in Eq. (10) denotes the iteration number, and the partial derivative terms in Eq. (10) are approximated according to the procedure outlined in Eq. (12) :

$$\frac{\partial y}{\partial x} \cong \frac{y(x + 1\%x) - y(x)}{1\%x} \tag{12}$$

In other words, calculations are taken for a given iteration, as well as 101% of the value of that iteration, and the diference is used to approximate the partial derivative.

**2.3. Experimental Apparatus and Procedure**

Two firing tests were carried out on a 30N-thrust class motor. A summary of the test conditions is listed in Table 2. A depiction of the test setup is shown in Fig. 4, and detailed schematics of the nozzle and fuel grain are shown in Figs. 5 and 6, respectively. Gaseous oxidizer was supplied from a single tank, and flow was controlled by a solenoid valve and air actuator. Oxidizer mass flowrate $\dot{m}_{ox}$ in units of kg/s was determined by using a small orifice plate to choke the flow, measuring the temperature and pressure of oxidizer upstream of the orifice ($T_{up}$ and $P_{up}$ in units of K and Pa, respectively) and carrying out the calculation in Eq. (13) :

$$\dot{m}_{ox} = C_{or} \left( \frac{\pi}{4} D_{or}^2 \right) \sqrt{\left( \frac{\gamma_{ox}}{R_{ox} T_{up}} \right) \left( \frac{2}{\gamma_{ox} + 1} \right)^{\frac{\gamma_{ox}+1}{\gamma_{ox}-1}}} P_{up} \tag{13}$$

where $D_{or}$ = 1E-3 is the orifice diameter in units of m, $\gamma_{ox}$ = 1.395 is the specific heat ratio of oxygen, $R_{ox}$ = 259.8 is the gas constant of diatomic oxygen in units of J/kg-K. Orifice discharge coefficient $C_{or}$ = 0.98 was determined experimentally.

Ignition was achieved by sending an electrical current through a coil of Nicrome wire affixed to the lip of the first fuel block using 1 g of epoxy (just downstream from the injector). Wire leads were fed through the nozzle exit and attached to a DC voltage source. Nicrome wire was heated for 10 s before actuating the oxidizer supply valve and initiating the firing test. Upon completing each firing test, the chamber was purged with gaseous nitrogen, both to extinguish the combustion of fuel and to cool the nozzle. High density polyethylene (HDPE) was used as the fuel, and grains were assembled from eight short cylindrical blocks. After assembly, fuel grains were loaded into glass fiber-reinforced plastic (GFRP) insulating tubes and sealed in a steel motor case. The nozzles were manufactured using the isotropic graphite Tokyo Tokai Carbon Ltd. G347 [12]. In order to reduce the heat transfer from the fore-end surface in the axial direction, the surface of the nozzle was made as a separate piece with the expectation that the discontinous surface contact would act as a sort of insulation. The seem where the two pieces meet is visible in Fig. 5.

Multiple dynamic and static measurements were taken during the experiments conducted in this study.

This document is provided by JAXA.

Pressures were measured using KYOWA DCS-10 MPa and KYOWA DCS-5 MPa pressure sensors with rated accuracies of ±0.040 MPa and ±0.028 MPa, respectively. Thrust was measured using a KYOWA LMB-A-200N load cell with a rated accuracy of ±3.5 N. Nozzle temperatures were measured using RC Pro k-type thermocouples rated up to a maximum temperature of 1100 °C. As a precautionary measure, all pressure sensors were tested simultaneously against the same source before each experiment to ensure that there were no abnormalities, and the load cell and thermocouples were tested for a response. Furthermore, due to the low level of thrust (<30 N) produced by the motor in the small-scale static firing tests, a preload of around 40 N was applied to the injector plate using two short bungee cords. Dynamic measurements were recorded at 200 Hz using DCS-100A series software, and later filtered using a 20-point moving average. The reason for applying a moving average was to reduce the presence of oscillations in reconstructed nozzle-throat-erosion histories.

Initial and final nozzle throat diameter measurements were taken by analyzing digital scans of the nozzle before and after firing. These scans were taken on an Epson GT-S600 series scanner at a resolution of 2400 DPI. A length scale was established for the scan by placing a plaque of 1 mm spacing grid paper next to the nozzle being scanned, and the nozzle was back lit to distinguish the rim of the throat surface from the background. The nozzle throat diameter was computed based on the area of the lighted region at the throat using an Excel spreadsheet function.

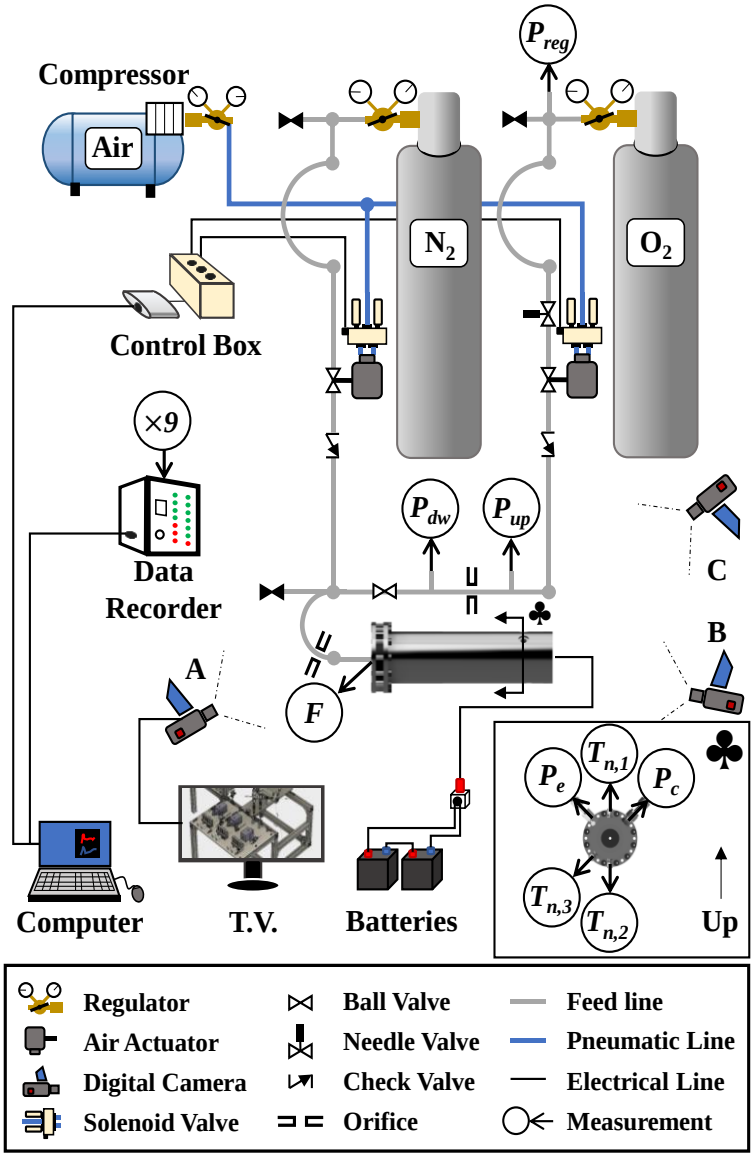


Fig. 4. Test Setup

This document is provided by JAXA.

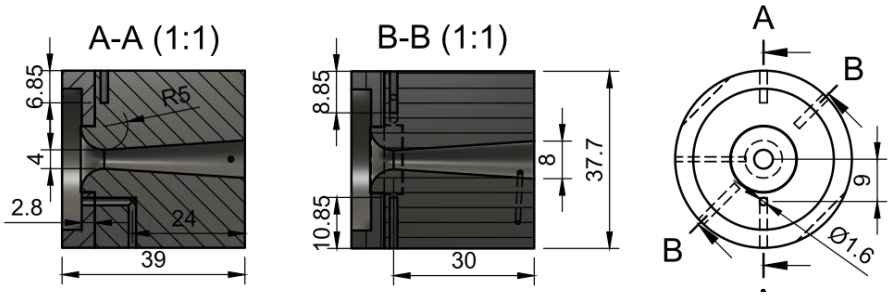


Fig. 5. Nozzle schematic

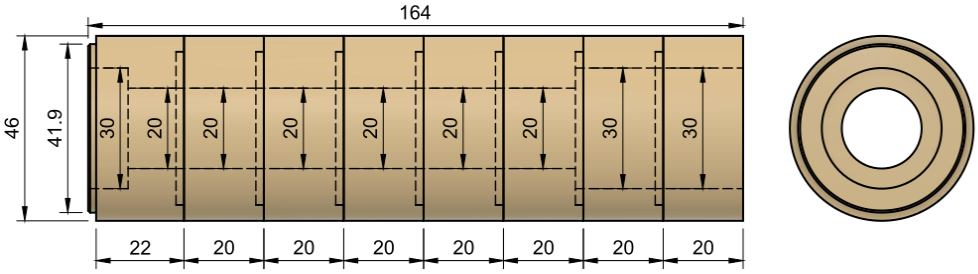


Fig. 6. Fuel grain schematic

Table 2. Summary of Test Data

| Term | $t_b$ | $\Delta M_{fu}$ | $\Delta D_t$ | $\bar{\dot{m}}_{ox}$ | $\bar{P}_c$ | $\bar{F}$ | $\bar{T}_{n1}$ | $\bar{T}_{check}$ | $\bar{T}_{n2}$ |
|---|---|---|---|---|---|---|---|---|---|
| Units | s | kg | m | kg/s | Pa | N | K | K | K |
| Test 1 | 4.95 | 14.4E-3 | 0.05E-3 | 11.1E-3 | 1.4 E6 | 23.5 | 706 | 585 | 541 |
| Test 2 | 4.92 | 18.0E-3 | 1.00E-3 | 14.8E-3 | 1.6 E6 | 33.7 | 827 | - | 575 |

Note : $T_{n1}$, $T_{check}$, and $T_{n2}$ were located 5mm, 8mm and 10mm from the nozzle throat

## 3. RESULTS AND DISCUSSION

### 3.1. Temperature Profile and Wall Temperature History the Nozzle Throat

A summary of analysis results is shown in Table 3. The temperature profiles for Tests 1 and 2 are plotted in Figs. 7 and 8, respectively, at one second increments. A third thermocouple inserted to a depth between thermocouples 1 and 2, listed as $T_{check}$ in subsequent sections, was used to check the accuracy of the profiles in Test 1. The calculated profiles were within less than 5% of the check value at all times in Test 1, validating the assumption in the governing equations of one-dimensional radial heat transfer at the throat. Since no nozzle erosion occured in Test 1, the consideration of chemical heat flux was not necessary. A check value was used in Test 2 as well, but the thermocouple was not inserted properly and this validation was not possible. Figures 9 and 10 plot the temperature histories of the boundary conditions in Eq. (5) – i.e. the combustion gas temperature and the thermocouple temperature $T_{n2}$, as well as the results for the throat wall temperature histories with their corresoponding experimental uncertainty for Tests 1 and 2, respectively.

### 3.2. Heat Flux at the Nozzle Throat

The maximum nozzle throat wall temperature in Test 1 was roughly 1800 K whereas the maximum in Test 2 was roughly 2400 K, an increase of >30%, even though the combustion gas temperatures in both tests were relatively unchanged. In following, the heat transfer rate to the nozzle must have been much larger in Test 2 than in Test 1. Figure 11 plots the histories of heat transfer coefficient factor $\zeta$ from both tests. In Test 1 the value of $\zeta$ reaches unity at around 2 s into the firing, and remains around unity for the duration of firing. This means that the Bartz correlation prediction matches our experimental results in Test 1. In Test 2 the value of $\zeta$ surpasses unity at around 1.5s into the firing, and continues to increase throughout the firing to a value over 2 times the value predicted by the Bartz correlation. Moreover, nozzle throat erosion becomes measureably large at around 1.75 s into the firing, resulting in an average throat erosion rate of $\bar{\dot{r}} = 0.5/3 = 0.17$ mm/s. This level of nozzle erosion leads to an observable increase in surface roughness at the throat, which is not a factor

This document is provided by JAXA.

in the Bartz equation. In following, it is important to point out that even though the nozzle erosion rate was considerably high, the magnitude of the resulting chemical heat flux was less than 2% of the values of conductive and convective heat fluxes. This is shown in Fig. 12 which plots the histories of heat flux in Test 2. Thus, it is reasonable to conclude that the high heat transfer rates observed in Test 2 are the result of an increase in surface roughness, and therefore the Bartz correlation cannot accurately predict this heating rate.

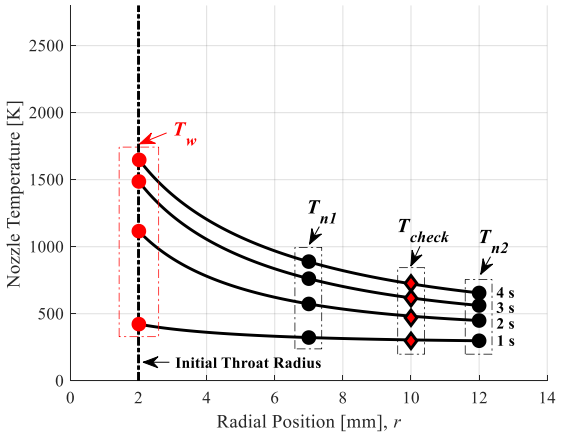


Fig. 7. Temperature profile in Test 1

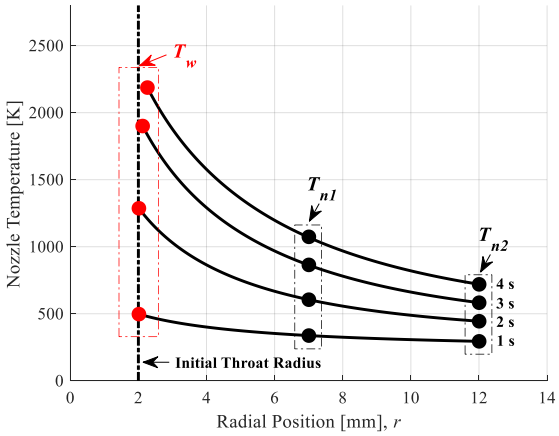


Fig. 8. Temperature profile in Test 2

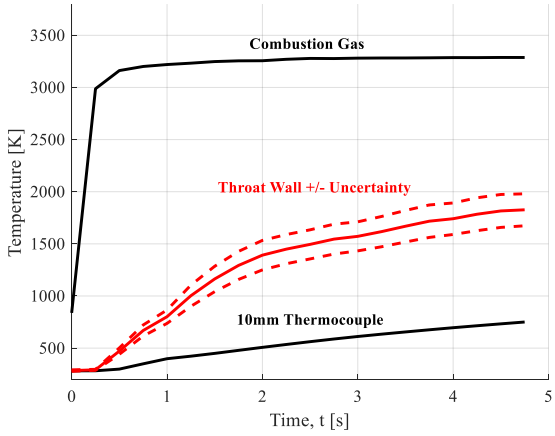


Fig. 9. Temperature histories in Test 1

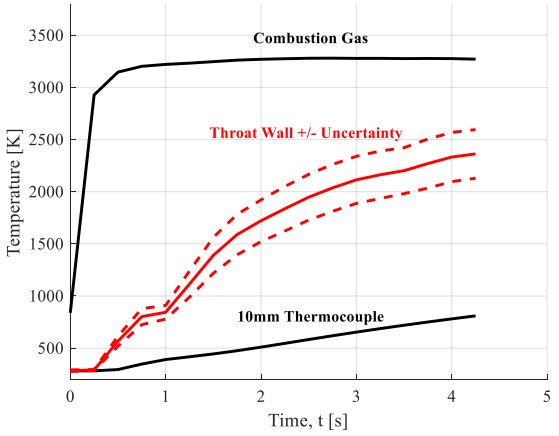


Fig. 10. Temperature histories in Test 2

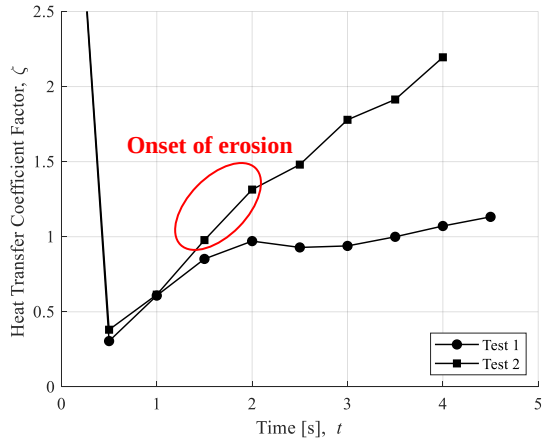


Fig. 11. The Bartz correlation underpredicts heat transfer coefficient in nozzle erosion case (Test 2).

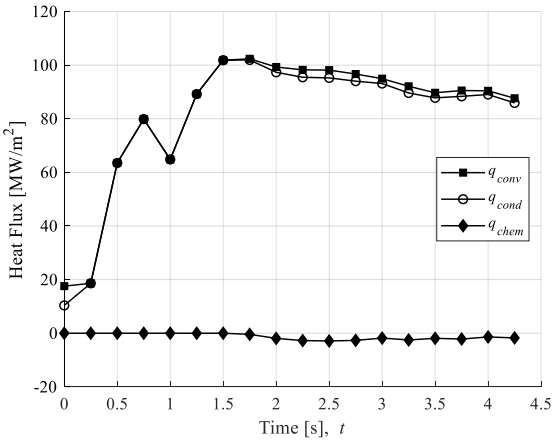


Fig. 12. Chemical heat flux negligible in Test 2

This document is provided by JAXA.

Table 3. Summary of Analysis Results

| | $t_{ero}$ | $\bar{\zeta}$ | $\bar{\theta}$ | $\bar{\phi}$ | $\bar{h}$ | $\bar{T}_g$ | $\bar{\dot{q}}_{conv}$ | $\bar{\dot{q}}_{cond}$ | $\bar{\dot{q}}_{chem}$ |
|---|---|---|---|---|---|---|---|---|---|
| | s | | | | W/m$^2$-K | K | W/m$^2$ | W/m$^2$ | W/m$^2$ |
| Test 1 | - | 0.9 | 0.4 | - | 42997 | 3394 | 7.79E7 | 7.79E7 | - |
| Test 2 | 1.75 | 1.3 | 0.5 | 0.009 | 64311 | 3392 | 8.58E7 | 8.45E7 | -1.30E6 |

Note : $T_{n1}$, $T_{check}$, and $T_{n2}$ were located 5mm, 8mm and 10mm from the nozzle throat

## 4. CONCLUSION

A new method for estimating nozzle throat wall temperature history in hybrid rocket firing tests is introduced with the aim of enabling experimental research on thermochemical nozzle erosion. This method builds off of a recently reported technique for determining nozzle throat erosion history and mixture ratio history in hybrid rocket firing tests, referred to as the Nozzle Throat Reconstruction Technique or NTRT, and thus this study is one of the first of its kind. The results of two static firing tests demonstrate that time histories of nozzle temperature profiles can accurately be reconstructed. Furthermore, this study reveals that the Bartz correlation may not be appropriate for predicting the convective heat transfer coefficient when nozzle throat erosion is taking place due to the effect of chemical erosion on the nozzle surface roughness – likely increasing turbulence and diffusion in the boundary layer.

## ACKNOWLEDGEMENTS

This research is supported by the Ministry of Education, Science, Sports and Culture, Grand-in-Aid for Science Research (B). 15H04197, 2016 and Grant-in-Aid for JSPS Fellows 18J2087708.

## REFERENCES

[1] Kuo, K., Chiaverini, M., “Hybrid Rocket Propulsion in 21st Century,” Fundamentals of Hybrid Rocket Propulsion, edited by Chiaverini, M. and Kuo, K., Progress in Astronautics and Aeronautics, AIAA, Washington, DC, 2006, pp. 593-638.

[2] Bianchi, D., Nasuti, F., “Numerical Analysis of Nozzle Material Thermochemical Erosion in Hybrid Rocket Engines,” Journal of Propulsion and Power, Vol. 29, No. 3, 2013, pp. 547-557.

[3] Kamps, L. T., Saito, Y., Kawabata, R., Wakita, M., Totani, T., Nagata, H., “Method for Determining Nozzle-Throat-Erosion-History in Hybrid Rockets,” Journal of Propulsion and Power, Vol. 33, No. 6, 2017, pp. 1369-1377.

[4] McDonald, A., Hedman, P., “Erosion of Graphite in Solid-Propellant Combust Gases and Effects on Heat Transfer,” AIAA Journal, Vol. 3, No. 7, 1965, pp. 1250-1257.

[5] Acharya, R., Kuo, K., “Effect of Pressure and Propellant Composition on Graphite Rocket Nozzle Erosion Rate,” Journal of Propulsion and Power, Vol. 23, No. 6, 2007, pp. 1242-1254.

[6] Thakre, P., Yang, V., “Chemical Erosion of Refractory-Metal Nozzle Inserts in Solid-Propellant Rocket Motors,” *Journal of Propulsion and Power*, Vol. 25, No. 1, 2009, pp. 40-50.

[7] Bartz, D. R., “A Simple Equation for Rapid Estimation of Rocket Nozzle Convective Heat Transfer Coefficients,” *Journal of Jet Propulsion*, Vol. 27, No. 1, 1957, pp. 49-53.

[8] Gordon, S., McBride, B., “Computer Program for Calculation of Complex Chemical Equilibrium Compositions and Applications,” NASA RP-1311, 1994.

[9] Lutcov, A. I., Volga, V. I., Dymov, B. K., “Thermal Conductivity, Electric Resistivity and Specific Heat of Dense Graphite,” Carbon, Vol. 8, 1970, pp. 753-760.

[10] Butland, A. T. D., Maddison, R. J., “The Specific Heat of Graphite: An Evaluation of Measurements,” Journal of Nuclear Materials, Vol. 49, 1973, pp. 49-56.

[11] “NIST-JANAF Thermochemical Tables,” Accessed Online <https://janaf.nist.gov> , 25th May 2018.

[12] “ISOTROPIC GRAPHITE:Typical properties,” Accessed Online <https://www.tokaicarbon.co.jp/en/products/fine_carbon/pdf/Isotropic_graphite.pdf> , 13th June 2018.

This document is provided by JAXA.